Simulation of Flow in the Silk Gland

ARTICLE *in* BIOMACROMOLECULES · DECEMBER 2008

Impact Factor: 5.75 · DOI: 10.1021/bm800752x · Source: PubMed

3 AUTHORS, INCLUDING:

David N Breslauer
Bolt Threads
10 PUBLICATIONS **728** CITATIONS
SEE PROFILE

Luke P Lee
University of California, Berkeley
303 PUBLICATIONS **9,944** CITATIONS
SEE PROFILE

Simulation of Flow in the Silk Gland

David N. Breslauer,*,† Luke P. Lee,†,‡ and Susan J. Muller†,§

UCSF/UC Berkeley Bioengineering Graduate Group, Bionanotechnology Center, and Department of Chemical Engineering, University of California, Berkeley, Berkeley, California

Received July 7, 2008; Revised Manuscript Received October 13, 2008

Spiders and silkworms employ the complex flow of highly concentrated silk solution as part of silk fiber spinning. To understand the role of fluidic forces in this process, the flow of silk solution in the spider major ampullate and silkworm silk glands was investigated using numerical simulation. Our simulations demonstrate significant differences between flow in the spider and silkworm silk glands. In particular, shear flow effects are shown to be much greater in the spider than the silkworm, the silkworm gland exhibits a much different flow extension profile than the spider gland, and the residence time within the spider gland is eight times greater than in the silkworm gland. Lastly, simulations on the effect of spinning speed on the flow of silk solution suggest that a critical extension rate is the initiating factor for fiber formation from silk solution. These results provide new insight into silk spinning processes and will guide the future development of novel fiber spinning technologies.

Introduction

Spiders and silkworms are able to produce silk fibers with minimal energy expense that outperform most other fibers in mechanical testing.[1] To understand how these exceptional fibers are produced so easily, the spinning mechanisms of silk glands have been under intense investigation.[1−4] Despite fundamental differences in the composition and structure of spider major ampullate (MA) and silkworm fibroin proteins,[5] the silk glands of both organisms have been shown to function similarly, by establishing an extremely complex regulatory environment for the conversion of the silk protein solution ("dope") into a solid fiber.[1] Simplistically, in both the spider MA gland and the silkworm, highly concentrated silk fibroin flows through the contracting geometry of the silk gland and is exposed to ionic gradients that regulate its crystallized state by inducing protein conformational changes and aggregation.[1,3] The silk dope eventually reaches a point of sufficient solidification that it detaches from the walls of the gland and is drawn out as a fiber. Whereas the molecular chemistry and structure of silk proteins and the effects of various ions on the folded state of silk fibroin have been thoroughly investigated,[5−7] the effects of flow on silk fiber formation have received relatively little attention.

It has long been known that silk fibroin exhibits unique responses to fluidic forces. These responses include varying liquid crystalline textures,[8,9] non-Newtonian flow profiles,[10,11] and flow-induced crystallization.[10,12−14] In particular, both dilute and concentrated silk fibroin have been shown to exhibit shear-thinning behavior,[11,15,16] whereby the viscosity of the solution decreases as a function of increasing imposed shear rate. Essentially, the shear field stretches the long, deformable molecules and distorts the molecular orientations and conformations; the viscosity decreases as increasingly higher shear rates result in increasingly disturbed distributions of conformations and orientations.[17] Furthermore, silk fibroin exhibits flow-induced crystallization,[10,12−14] during which the stretching of polymer molecules in flow creates a favorable state for crystal formation. It has been shown that silk fibroin begins crystallizing after exposure to a critical shear rate.[11,12] To this end, shear rate profiles along the silkworm gland have been mapped to determine how flow in the gland induces fiber formation.[12,18]

The silk gland in the silkworm and the spider MA gland are both decreasing diameter funnels, whose shapes fit well to a two-stage exponential function.[3,9] It has been noted that similar hyperbolically shaped funnels are used in industry to spin commercial fibers,[1] and it has been proposed that this shape could cause a slow elongation of the silk fibroin molecules, stretching and aligning them along the final fiber axis, as well as inducing crystallization.[9] Considering the importance of fluidic forces on the flow and crystallization of silk fibroin, it is very likely that the geometry of the gland plays an important role in the fiber spinning process. Leveraging the recent viscosity measurements of Kojic et al.[16] and previously published data on the geometry of the *Nephila edulis* MA and *Bombyx mori* silk glands,[3,9] we have performed finite element method simulations (FEMs) of the non-Newtonian flow in the silk gland of both organisms to further elucidate the role of the flow on the formation of silk fibers.

Methods Section

Data Acquisition. The shape of the *Nephila edulis* MA silk gland was obtained from Knight et al.[9] and the shape of the *Bombyx mori* silk gland from Asakura et al.[3] Data points were manually extracted from the figures using the GRABIT software[19] in MATLAB 2007 (Mathworks, Inc.). For each figure, data was extracted three times, and the values averaged. The radius (r, in μm) of each gland as a function of axial position (z, in μm) was fit to a two-stage exponential function ($r(z) = ae^{bz} + ce^{dz}$) using the MATLAB curve-fitting toolbox. For the spider, $a = -0.004886\ \mu$m, $b = 0.0003718\ \mu\text{m}^{-1}$, $c = 53.52\ \mu$m, and $d = -9.989 \times 10^{-5}\ \mu\text{m}^{-1}$ ($R^2 = 0.9735$). For the silkworm, $a = 139.8\ \mu$m, $b = -0.00197\ \mu\text{m}^{-1}$, $c = 58.45\ \mu$m, and $d = -3.58 \times 10^{-5}\ \mu\text{m}^{-1}$ ($R^2 = 0.9824$).

The resultant curves were calculated every 100 μm, and this data was imported into AutoCAD 2006 (Autodesk) and connected as a polyline. Curves were subsequently imported into COMSOL Multiphysics 3.4 (COMSOL AB) as axisymmetric structures.

Numerical Simulation. Finite element simulations were performed using the COMSOL Non-Newtonian Fluid Flow solver. All simulations

* To whom correspondence should be addressed. E-mail: davidb@berkeley.edu.
† UCSF/UC Berkeley Bioengineering Graduate Group.
‡ Bionanotechnology Center.
§ Department of Chemical Engineering.

10.1021/bm800752x CCC: $40.75
Published on Web 11/24/2008

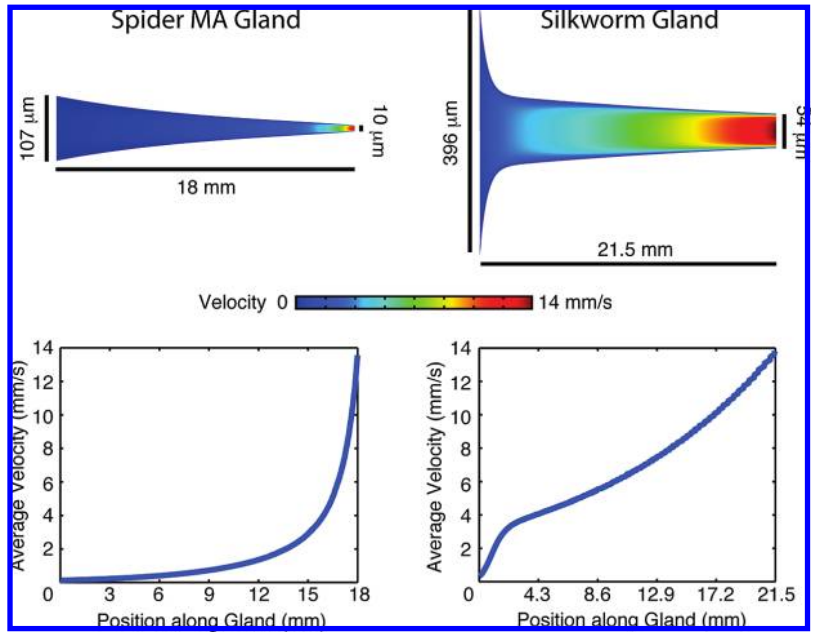

Figure 1. Magnitude of the velocity vector (top) and cross-sectionally averaged total velocity (bottom) along the MA silk gland of the spider (left) and silkworm silk gland (right). Note the difference in scale between the radial and the axial axes.

were isothermal. Geometry meshes were automatically generated by COMSOL. Because of the high length-to-width aspect ratio of the structures, the radial axis was scaled up five times before meshing and subsequently rescaled to its original size. Typical meshes contained approximately 15000 elements.

Viscosity data for the native *Nephila clavipes* (MA gland) and *Bombyx mori* silk solutions were obtained from Kojic et al.[16] It should be noted that the obtained geometry is from the *Nephila edulis* spider and the obtained viscosity data from the *Nephila clavipes* spider. However, the two different species are often studied interchangeably.[1] Kojic et al. fit their viscosity data to a Carreau−Yasuda viscosity model, which adequately captures the observed zero-shear rate plateau regime and shear-thinning behavior of silk solutions. However, the rheology of liquid crystalline solutions is quite complex, as it is usually coupled with the development of liquid-crystalline textures and requires multiple viscosity coefficients for an adequate description of flow behavior.[17,20] Other models, such as the Leslie−Ericksen theory for the viscous stress of nematics, could be more relevant, by including the effects of molecular alignment on stress.[17,20] Until studies are available that correlate the molecular alignment, structure, and rheological behavior (i.e., that specify the values of the multiple material constants in the Leslie−Ericksen theory), we are limited to simplified models of the flow of silk secretions.

The Carreau−Yasuda model describes non-Newtonian viscosity by

$$\eta(\dot{\gamma}) = \eta_0[1 + (\dot{\gamma}\lambda)^a]^{(n-1)/a}$$

where η is viscosity as a function of shear rate $\dot{\gamma}$, η_0 is the zero-shear viscosity, λ is a relaxation time of the fluid, a represents the rate of transition from zero-shear viscosity to shear-thinning behavior, and n is the exponent characterizing the shear-thinning regime. For *Nephila clavipes*, Kojic et al. found $\eta_0 = 3500$ Pa·s, $\lambda = 0.40$ s, $a = 0.68$, and $n = 0.18$. For *Bombyx mori*, they found $\eta_0 = 5200$ Pa·s, $\lambda = 0.57$ s, $a = 0.80$, and $n = 0.17$. These values were measured from silk secretions gathered from the storage sac of a spider MA gland and a silkworm gland, restricting the rheological data to solutions from those areas, and not necessarily representing changes in microstructure that develop along the length of the gland. Furthermore, Kojic et al. extracted silk secretions in distilled water for approximately 5 min, which could potentially alter the structure and rheology of the silk dope. We note that no data on fluid elasticity is available for either solution, so non-Newtonian effects are restricted to those associated with shear-thinning of the viscosity. The density of natural silk secretion was assumed to be 1.15 g/cm^3.[21]

The gland wall was specified to have a no slip boundary condition. Silkworms, however, are known to secrete another protein, sericin, around their silk secretions as it flows through the silk gland.[5,22] Whereas sericin acts as glue in the formation of the cocoon, it is also believed to act as a lubricating layer in the silk gland, reducing the pressure drop required for flow.[16,22] Due to the technical challenges associated with modeling a two-phase flow, particularly in the absence of rheological characterization of the sericin layer, we are ignoring the presence of sericin and its effects on flow.

Gland entrance and exits were specified to have inlet pressure and outlet pressure boundary conditions, respectively. To achieve the desired outlet flow rate, the inlet pressure was iteratively adjusted until the outlet flow rate was approximately as desired. For all simulations, values for conservation of mass and mesh convergence were checked to be within 5%. Mesh convergence was checked for conservation of mass at the inlet and outlet, as well as at nodal values for velocity along the gland length.

Results and Discussion

Velocity Along the Silk Gland. Figure 1 shows the velocity profile along the *Nephila* MA and *Bombyx* silk glands when a fiber is drawn at physiological spinning rates (10−20 mm/s).[1,23] For these rates, the Reynolds' number (Re) in the gland is small (Re $\ll$ 1), indicating that the flow is laminar (Table 1). The color map indicates the magnitude of the velocity vector; in the lower figure the cross-sectional average total velocity is shown as a function of axial position along the gland (of course, because we are averaging over a cross-sectional surface whose normal points in the axial direction, only the axial velocity component contributes to the average). Henceforth, total velocity refers to the magnitude of velocity vector (accounting for both axial and radial components).

Despite the glands of each organism fitting well to a two-stage exponential function, their shapes are quite different. The spider MA gland has a slow and steady decrease in radius, whereas the silkworm gland has a more sudden drop, and then a slow decrease in radius. This difference in shape induces quite

Table 1. Simulation Parameters and Results[a]

	Re	inlet velocity (mm/s)	outlet velocity (mm/s)	pressure drop (Pa)	residence time (s)
Nephila	4.92×10^{-9}	0.140	13.7	5.40×10^{7}	38.6
Bombyx	2.92×10^{-8}	0.334	13.8	3.09×10^{7}	4.79

[a] Inlet and outlet velocities are cross-sectional averages of the total velocity along the boundary. The Reynolds' number here is defined as $\mathrm{Re} = \rho V d/\eta_0$, where ρ is the fluid density, V is the average velocity at the inlet, d is the diameter at the inlet, and η_0 is the zero-shear rate viscosity defined in the text.

different average velocity profiles along the glands (Figure 1). In the spider, the velocity increases at a low rate and then rises dramatically with axial distance along the gland. A similar velocity profile was obtained by Kojic et al. from a mass balance-based numerical simulation of a uniformly moving cross section of silk through the *Nephila clavipes* MA gland.[24] In the silkworm, however, there is an initial rapid increase in velocity followed by a much slower rate of increase along the gland. The pressure drops required to produce these physiological velocity profiles are on the same order as previously published results of 40 and 50 MPa for the spider[16] and silkworm,[18] respectively. The pressure values from previous reports were also obtained from simulations of silk fibroin flow in the gland. The values, however, are theoretical only, and are used to mimic the tension exerted on the dope during the drawing of a silk fiber. Accurate measurements of physiological spinning speeds and tensions have been performed for the vertical fall of a spider.[25] These measurements revealed that physiological spinning speeds range from 0.05 to 1.30 m/s and physiological drawing tensions range from 10 to 20 MPa on the fiber. For a 3 μm diameter fiber, that is $\sim$8 μm in diameter within the gland, these tensions correspond to a tension in the silk gland of $\sim$1.1 to 2.2 MPa. Based on these considerations, we repeated our simulations on the spider MA gland with an applied pressure drop of 1.7 MPa to report more physiologically relevant results. The applied pressure drop corresponds to an outlet velocity of 3.65 μm/s, well below the measured range, as well as a highly unreasonable fluid particle residence time of 1.51×10^5 s. The latter value demonstrates the limitations of such simplified simulations. It is likely that additional lubrication layers in the silk glands (see Methods Section) lead to the low physiological drawing tension, and cause the same applied tension to be too low to produce realistic results.

From the long and slender contraction geometry of both silk glands, one would expect to be able to approximate the flow behavior with a lubrication theory model of flow in a tapered channel. This problem has been previously solved for both Newtonian and Power Law fluids in linearly tapered tubes.[26] However, this analytical lubrication theory approximation (treating the gland as having a linear taper) of Newtonian flow in the spider MA gland underestimates the necessary pressure drop by over 25%, in comparison to a Newtonian simulation. The error increases further when additionally attempting to account for non-Newtonian flow behavior, or when analyzing the silkworm silk gland, which has a much sharper taper than that of the spider MA gland. Therefore, the published analytical lubrication model does not serve as an accurate approximation of flow behavior in the silk glands and should be applied with caution.

Figure 2 shows profiles of total velocity as a function of radial position at various positions along the gland length. Whereas the plots are of total velocity, axial velocity plots look identical because the relative magnitude of the radial velocity is much smaller than the axial velocity. Because the silk solution is highly shear thinning, the cross-sectional velocity profile forms a highly blunted flow profile, rather than the commonly seen

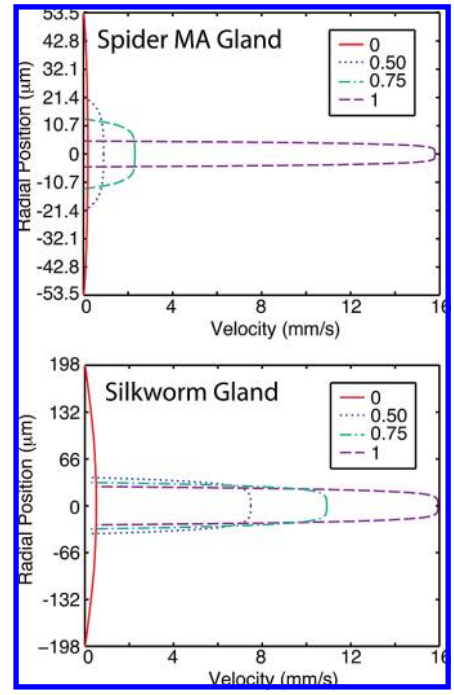

Figure 2. Radial cross-section velocity profiles at various positions along the gland lengths, indicated in the legend by axial position scaled by the total gland length. (top) Spider gland, (bottom) silkworm gland. The blunted shape of the velocity profiles is due to the shear-thinning behavior of the silk solution.

parabolic velocity profile of Newtonian Poiseuille flow. Due to this thin high shear rate layer, the flow at any axial position in the gland is essentially a plug flow. This shear-thinning behavior has a significant beneficial effect on the pressure drop required to flow silk solution.

For example, if the silk solution were a Newtonian fluid, and not shear thinning, the pressure drop required to flow the solution at the same rate would be 2 orders of magnitude higher for both the spider and the silkworm (determined by simulation of the flow as a Newtonian fluid with the zero-shear viscosity as the Newtonian viscosity). Therefore, the shear-thinning character of the silk solution, also a feature of most other liquid crystalline polymers,[17,20] greatly facilitates low energy fiber spinning.

Residence Time in the Gland. From the velocity profile along the length of the gland, we calculated the mean residence time of a fluid particle in the gland. Residence time (t_{res}) is the amount of time that a particle is exposed to the imposed flow field, and is herein defined by

$$t_{res}(z) = \int_0^z \frac{dz}{V_{avg}(z)}$$

where V_{avg} is the cross-sectional average of the velocity at a position along the gland, z. It is known that although extendable molecules show a stochastic distribution of stretching in both shear and extensional flow fields, their residence time is positively correlated to the amount of stretching of the molecules.[27,28] Consequently, the longer a fibroin molecule is

in the gland, the more elongated and aligned it will be along the gland axis. Our calculations (Table 1) indicate that silk dope in the spider MA silk gland has a residence time eight times longer than silk dope in the silkworm gland. This is particularly noteworthy considering that both glands are of similar lengths, and with the same approximate inlet and outlet velocities. Reexamining the velocity profiles along the gland (Figure 1), the extended residence time in the spider is due to the much slower fluid acceleration along the gland.

Both the spider and silkworm maintain ionic gradients, as well as extract water from the silk solution, along the lengths of their glands.[7] A rough calculation of diffusion distance ($x = \sqrt{4Dt}$, where t is time and D is the diffusion coefficient) using the diffusion coefficient of water through native spider silk dope[24] ($D = 2.15 \times 10^{-5}$ mm^2/s) suggests that the short residence time in the silkworm does not leave enough time for complete diffusion of water or ions from the gland edge to the center of the dope. The longer residence time of the spider MA gland potentially allows much more judicious regulation of the water and ionic content of the silk dope. These diffusion calculations are approximate and obviously do not account for the effects of advection or, potentially, stress-induced diffusion.

Shear and Extension. To further understand the role of flow fields and hydrodynamic forces within the silk gland, we have plotted the magnitude of the rate of strain tensor and a flow type parameter throughout the flow fields as well as calculated characteristic shear rates and characteristic extension rates along the gland lengths. Roughly speaking, shear forces are a result of "sliding" of the silk solution against the gland wall, and extensional forces are a result of stretching along the flow axis. In particular, since the silk glands have a funnel shape, their decreasing diameter causes a spatial acceleration along the flow direction, stretching fluid particles. Combined with the shear effects at the gland wall, the silk gland creates a mixed shear and elongational flow. The elongational component has recently been demonstrated in vitro to be necessary for silk fiber formation.[29] Due to the complexities associated with each, shear and elongational flow are commonly analyzed independently.[30] However, their combined effect is of significant interest to the polymer rheology community because of its role in the dies used for polymer fiber spinning, extrusion, and other processing flows.[26,31]

A flow type parameter can be used to assess the relative proportion of the rotational and elongational components of a flow field. We plotted the dimensionless flow type parameter (ξ) for each gland, as previously defined[32]

$$\xi = \frac{|\underline{\underline{\dot{\gamma}}}| - |\underline{\underline{\omega}}|}{|\underline{\underline{\dot{\gamma}}}| + |\underline{\underline{\omega}}|}$$

where $|\underline{\underline{\dot{\gamma}}}|$ is the magnitude of the rate of strain tensor, and $|\underline{\underline{\omega}}|$ is the magnitude of the vorticity tensor. The flow type parameter varies from -1 (pure rotation) to 0 (shear) to 1 (pure elongation).

As seen in Figure 3 (top), the axial centerline of both silk glands contain purely elongational flow, as expected for a contraction geometry.[33] It is in this location that polymer molecules likely experience the most stretching. Farther from the axial centerline of the gland, the flow is predominately shear ($\xi \sim 0.2$) due to the no slip boundary at the gland wall. This is highlighted in the plots of the magnitude of the rate of strain tensor ($|\underline{\underline{\dot{\gamma}}}|$) in Figure 3 (bottom). In both glands, $|\underline{\underline{\dot{\gamma}}}|$ ranges over several orders of magnitudes with the rate of strain highest at the walls and closer to the gland outlet. As mentioned above and discussed further below, we do not model the flow of any fluid layers around the silk secretions (e.g., sericin). However, if sericin does indeed act as a lubricant in the silkworm silk gland, the rate of strain induced by the wall would likely be significantly reduced.

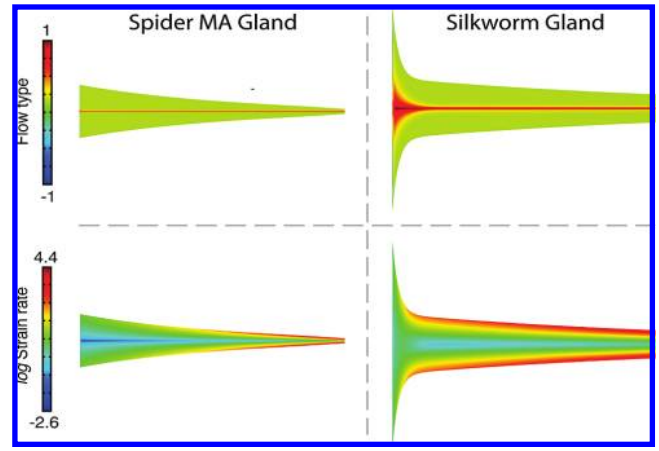

Figure 3. Flow type parameter (top) and magnitude of the rate of strain tensor (bottom) in the MA silk gland of the spider (left) and silkworm silk gland (right).

To provide a global description of flow in the glands, we calculated the characteristic shear rate ($\dot{\gamma}$) along the gland length as

$$\dot{\gamma}(z) = \frac{V_{avg}(z)}{r(z)}$$

and the accumulated shear strain (γ)

$$\gamma(z) = \int_0^{t(z)} \dot{\gamma}(z)\mathrm{d}t = \int_0^z \dot{\gamma}(z)\frac{\mathrm{d}z}{V_{avg}(z)}$$

where t is the total time of exposure to the flow field (i.e., residence time). Whereas shear rate describes the local rate of shear deformation, the accumulated shear strain is a function of both the magnitude of the shear field and the residence time within it.[26] As mentioned, both residence time and accumulated strain units have been shown to be positively correlated with the total amount of stretching of polymeric molecules,[27,28] and it has been demonstrated that repeated exposure of silk fibroin to identical shear fields induces irreversible changes in its material properties.[11] Finally, as suggested by Figure 2 and shown in Figure 3, we note that the local shear rate varies considerably with radial position, with the local shear rate going to zero at the centerline and reaching a maximum near the walls of the gland. Our characteristic shear rate, which neglects these radial variations, thus leads to an underprediction of the shear rate and shear strain experienced by near-wall fluid elements.

Like the velocity profiles for the two organisms, the characteristic shear rate profiles are distinctly shaped (Figure 4). However, the shear rate in the spider MA gland is an order of magnitude greater than that in the silkworm gland. Because the outlet velocities are approximately similar, this is primarily due to the small radius of the spider MA gland. Furthermore, the spider MA silk dope accumulates almost double the total average shear strain units of that of the silkworm before exiting the gland. In combination with the extremely long residence time of silk dope within the spider MA silk gland, the higher accumulated shear strain suggests that the slow stretching of the fibroin molecules over a long period of time could be a cause of different mechanical properties between spider MA silk fibers and silkworm silk fibers.

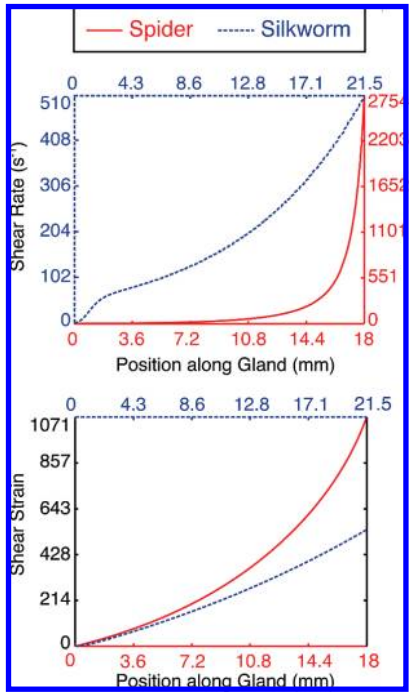

Figure 4. Characteristic shear rate (top) and characteristic accumulated shear strain (bottom) along the silk glands. Note the different scales for the characteristic shear rate in the spider MA and silkworm glands.

Our reported values of shear rates in the glands for both organisms are orders of magnitude higher than those generally discussed in the literature (the critical shear rate of fibroin crystallization is generally reported to be between 1 and 10 s^{-1}.[10−13,18,34]) This is largely due to our definition of shear rate, which is based on a radially averaged velocity profile, rather than fully accounting for the radial variations of shear rate. The FEM of the *Nephila clavipes* MA silk gland performed by Kojic et al.,[24] which is based on mass balance and neglects any radial variations in flow, suggests shear rates up to ~1500 s^{-1} at the outlet, on the same order as those reported here for the same gland. (Shear rates were not explicitly calculated in their report; rather, we performed the calculations based off their reported velocities and geometries.) Moriya et al.[18] performed an FEM simulation of flow in the silkworm gland based on their own viscosity and shear rate measurements. They reported shear rates of 0−2.5 s^{-1} along the centerline of the silkworm gland, but did not explicitly discuss details of differences between local and global flow kinematics. However, our simulations of the silkworm gland suggest similar local, centerline strain rates ranging from 0.5 to 3.5 s^{-1}.

We define the characteristic extension rate ($\dot{\varepsilon}$) by

$$\dot{\varepsilon}(z) = \frac{dV_{center}(z)}{dz}$$

where V_{center} is the centerline axial velocity of the fluid at a position, z. Although the cross-sectional average axial velocity is used in the definition of shear rate, the centerline axial velocity is conventionally used in characterizing extensional flows in converging channels[33,35,36] (further justified by the fact that the centerline is the location of pure elongational flow, Figure 3). We define accumulated extensional strain (ε)

$$\varepsilon(z) = \int_{t(z_0)}^{t(z)} \dot{\varepsilon}(z)dt = \int_{z_0}^{z} \dot{\varepsilon}(z)\frac{dz}{V_{avg}(z)}$$

The onset of the polymer coil-to-stretch transition occurs above a critical extension rate ($\dot{\varepsilon}_{crit}$)

$$\dot{\varepsilon}_{crit} \approx \frac{0.5}{\lambda}$$

where λ is the polymer relaxation time.[26,27] Herein, we use the relaxation time from the Carreau−Yasuda model, as described above. Because polymer stretching only occurs above this critical rate, we have considered "useful" accumulated extensional strain by integrating only those areas of the extension rate curves above $\dot{\varepsilon}_{crit}$. In the silkworm gland, the extension rate profile is not monotonic, and falls above and below the critical extension rate (Figure 5). Whereas polymer relaxation could occur during the period of below-critical extension rate, negating the earlier effects of stretching, Holland et al. demonstrated that repeated shearing of silkworm dope caused an irreversible increase in the storage modulus of the dope, despite allowing >10 min for relaxation.[11,37] Therefore, in our calculation of "useful" accumulated extensional strain (above the critical extension rate), we sum the integrals of all useful extension.

From the extension rate profile (Figure 5), it is immediately obvious that neither silk gland is shaped as a constant extension rate funnel, as has been previously suggested for the spider MA gland.[1,9] Constant extension rate funnels have been under investigation in the fiber spinning community because they are believed to minimize the pressure drop required for flow as well as induce and maintain the highest degree of molecular alignment in a solution.[38−40] The spider MA gland actually acts as an increasing extension rate funnel, perhaps in order to maintain extension despite the strain hardening character of highly strained silk dope.[16]

The maximum extension rate in the spider silk MA gland rises to an order of magnitude higher than that in the silkworm gland. However, the extension rate in the silkworm gland exhibits a unique behavior. There is an initial spike and subsequent drop in extension rate (a "pre-extension") along the gland. Whereas the accumulated extensional strain in the spider

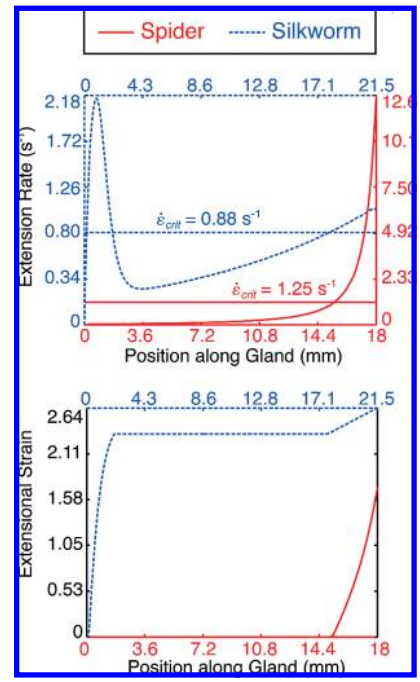

Figure 5. Characteristic extension rate (top) and useful accumulated extensional strain (bottom) along the silk glands. The horizontal lines indicate the critical extension rate for polymer stretching. Note the different scales for the characteristic extension rate in the spider MA and silkworm glands.

Table 2. Silk Dope Residence Time at Various Silking Speeds[a]

approximate drawing rate (mm/s)	residence time (s)	
	spider	silkworm
0.1	4790	548
15	38.6	4.72
50	10.2	1.29
100	5.16	0.643

[a] Drawing rates are approximate because pressure boundary conditions were applied in simulations. See Figure 6 legends for actual drawing rates.

MA gland is nearly linear, the aforementioned spike of extension rate in the silkworm gland manifests as an initial sudden rise in accumulated extensional strain. The total accumulated extensional strain in both the spider and silkworm is similar, despite the maximum extension rate in the spider MA gland being an order of magnitude higher than in the silkworm gland. The "pre-extension" enables the silkworm to achieve the same total accumulated extensional strain as the spider, at lower extension rates. Preshearing in the direction of polymer extension has been shown to more rapidly induce the onset of strain hardening.[41] Furthermore, the pre-extension could be a mechanism of achieving a higher total level of accumulated extensional strain despite the significantly shorter residence time of the silk dope in the silkworm gland. It is also noteworthy that both the spider MA and the silkworm glands accumulate similar magnitudes of total extensional strain, suggesting that accumulated shear strain is more important than extensional strain in the formation of spider dragline silk fibers.

In the spider MA gland, useful accumulated extensional strain begins near the end of the gland, around where the silk dope generally detaches from the gland wall and draws down into a fiber. Also, after a steady plateau of useful extension in the silkworm gland, useful extension begins to increase again similarly near the gland outlet. This suggests that critical extension rate and extensional strain may play a role in initiating drawdown and fiber formation in the glands. Notably, this area around the drawdown taper is the location of an abrupt increase in molecular alignment along the fiber axis, as measured by polarized Raman spectroscopy.[42]

Effects of Spinning Speed. Whereas the spider and silkworm normally spin silk in the range of 10−20 mm/s, forced silking is generally performed at a variety of different rates. These different drawing conditions of silk fibers have a significant effect on the mechanical properties of the resultant fibers.[43] It is unknown, however, exactly why spinning speed alters fiber properties, but it is likely due to the increased degree of molecular alignment induced by the stretching of the fiber (either during flow or postspin drawing) coupled, possibly, with decreased time for diffusion of water and ions. It has been observed that as draw rates are increased, the drawdown taper (the point at which the silk dope significantly solidifies and detaches from the gland wall) occurs at an earlier position within the gland.[3] Alongside this, similar shifts in the positions of maximum birefringence (and thus, molecular alignment) within the gland at various draw rates have been observed.[3,44] To investigate these effects, we performed simulations at spinning rates comparable to those used in forcible silking (0.1, 15, 50, and 100 mm/s). The results are shown in Table 2 and Figure 6.

It is believed that the drawdown taper begins when the silk dope is exposed to a critical shear rate, at which point a dramatic crystallization of the fibroin protein occurs.[3,18] In vitro experiments with native and regenerated silkworm fibroin suggest that this rate is within $1-10\ s^{-1}$.[10−13,18,34] Knight et al., from which we extracted the *Nephila* MA gland geometry, indicated that the drawdown taper occurred when the gland narrowed to 20 μm in diameter when drawing at 100 mm/s.[9] Our simulations of these conditions would thus suggest a critical shear rate of $\sim 2500\ s^{-1}$ (and a critical extension rate of $\sim 10\ s^{-1}$) for spider silk dope. As explained above, we believe this shear rate value to be considerably greater than measured critical shear rates due to the fact that our definition of characteristic shear rate incorporates the substantial radial variations in local shear rates. It is worth noting, however, that the centerline strain rate at this same axial location in the gland is $3\ s^{-1}$.

It is unclear to which flow characteristics the refolding and crystallization of silk fibroin is most responsive (e.g., deformation rate, accumulated strain, etc). Our simulations of different drawing rates show dramatically different residence times (Table 2) and shifts in magnitude of shear and extension rate profiles (Figure 6). On the other hand, accumulated shear strain is not significantly altered by drawing rate (data not shown). As draw rate increases in the spider MA gland, the location at which the extension rate reaches the critical value (and extensional strain becomes useful) moves farther back into the gland (Figures 6 and 7), similar to the shift in position of the drawdown taper at different spinning speeds, suggesting that surpassing the critical extension rate of the polymer molecules is the initiating factor for the drawdown taper. The silkworm gland exhibits a different extensional strain profile, whereby at drawing speeds significantly above physiological rate, all the extensional strain becomes useful (Figures 6 and 7). Similar to accumulated shear strain, accumulated extensional strain (when the entirety of the extension rate profile is above the critical rate) is not significantly altered by drawing rate (Figure 7). The lack of significant variation in accumulated shear strain and the aforementioned accumulated extensional strain for different drawing rates is expected because, as we have defined them, they are determined primarily by the geometry (as the integral of dz/r). However, because of shear-thinning, slight variations at different drawing rates may arise due to changes in the local strains near the wall.

Lastly, at the lowest drawing speed (0.1 mm/s), neither organism achieves extension rates above their respective critical values. However, fibers can obviously be artificially reeled at these speeds, albeit resulting in different mechanical properties than normal.[43] It is possible that, at this drawing rate, fiber formation occurs due to shear and ionic effects alone, with little polymer extension and alignment.

Limitations of Numerical Simulations. Many assumptions are inherent in performing these simulations on the spider MA and silkworm silk glands. Assumptions of considerable importance are as follows.

(1) *The silk secretions are considered homogeneous*. Despite the macroscale similarity between the rheological properties of the spider MA and silkworm dopes,[11] the two secretions have quite different molecular compositions that develop into different microstructures. *Nephila* MA silk secretions consist of two proteins, MaSp1 (~275 kDa) and MaSp2 (~740 kDa).[45−47] MaSp1 is most abundant in the dragline fiber, with MaSp2 heterogeneously distributed.[48] Both MaSp1 and MaSp2 contain polyalanine and glycine-alanine repeats, thought to form crystalline domains. MaSp2, however, contains significantly more proline than MaSp2, which is thought to confer much of the elasticity to the fiber. Silkworm silk secretions are composed of two proteins in a 1:1 ratio: a heavy chain (~390 kDa) and a light chain fibroin (~26 kDa) that are held together by a disulfide bond.[5] Silkworm fibroin amino acid sequences consist primarily of repeats of glycine alternating with alanine, serine, threonine,

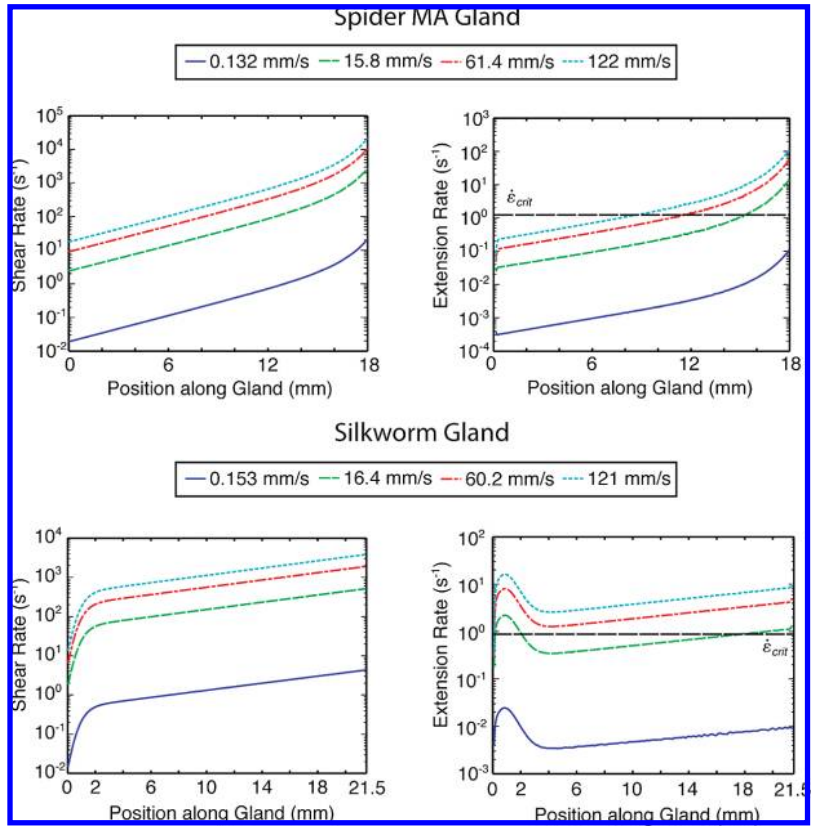

Figure 6. Effect of spinning speed on shear rate (left) and extension rate (right) profiles in the spider (top) and silkworm (bottom) glands. Legends indicate average exit velocities, representative of drawing rates. Note that the vertical axis is a logarithmic scale for visualization of the significant magnitude shifts.

and valine. These differences in molecular composition between spider MA and silkworm silk secretions can manifest as distinct microstructures and supra-molecular architectures, which we ignore in these simulations by only considering the rheological properties of storage sac silk secretions. Future work would benefit from the coupling of models describing the various hierarchies of molecular ordering and structure such as liquid crystal alignment and the development of mesogen structural morphology.[21,49−51]

(2) *Only the effects of shear-thinning of the viscosity are considered.* Neither elongational viscosity nor the effects of fiber solidification are taken into account. Whereas these factors are extremely important in polymer processing, they are difficult to both measure and model. Kojic et al. were able to use their specialized elongational rheometer to measure the elongational effects on native spider silk solution.[16] However, implementing their measurements into a numerical simulation remains a considerable challenge.

(3) *No slip boundary conditions are assumed at the gland wall*. Whereas we assume no-slip contact between the fluid and the gland wall, the exact interface boundary conditions are unclear.[1,16] For example, as the silk solution progresses down the gland, water diffuses out of the solution, potentially creating a lubrication layer at the gland wall. Furthermore, both the spider and silkworm have been shown to secrete additional lipid and protein layers in the glands,[1] which could induce varying interface flow effects between the silk solution and the gland wall. This is particularly likely in the secretion of the sericin protein in the silkworm gland, as discussed in the Methods Section.

(4) *Ionic effects on the viscosity of the silk solution are neglected*. The cells lining the walls of the silk gland regulate the ionic content of the silk solution and vary the ionic content along the gland length. It has been shown that these ions play a significant role in regulating the folding of the silk protein, as well as affecting the viscosity of the silk solution.[7,15,52,53]

(5) *Gland curvature is ignored*. The major and minor ampullate silk glands of the spiders are generally referred to as "S-shaped" because they wrap over themselves twice.[1] Silkworm glands also exhibit a similar shape. We neglect this curvature and consider the gland as a straight funnel to simplify axisymmetric simulations. It is possible, however, that the different radii of curvature at the inside and outside of these bends induce additional strain in the flow or even secondary flows.[54−56] Compared to the length scale of the entire gland and the total strain accumulated along its length, any additional extension induced by the bends is likely minimal.

(6) *The arbitrary nature of selecting the gland geometries*. Because the gland shapes were extracted from previously published data,[3,9] there is uncertainty as to whether the lengthwise bounds of the simulated geometries are representative of the physiologically relevant gland boundaries. Particularly in the case of the silkworm, the entirety of the gland extends much farther back than the simulated geometry and actually consists of two ducts that converge into the one duct analyzed herein. This leaves open to question the role of flow in those additional areas and their upstream effects.

Conclusions

The flow fields in the spider MA and silkworm silk glands were investigated through FEM simulations. Our results demonstrate that the shear-thinning behavior of natural silk secretions considerably assists in the low-pressure silk fiber spinning

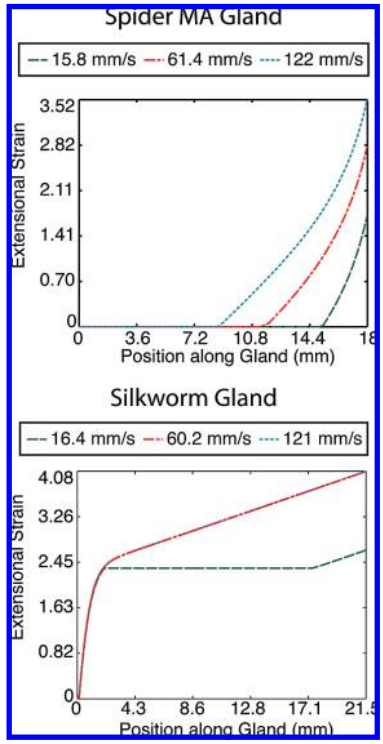

Figure 7. Useful accumulated extensional strain in the spider MA gland (top) and silkworm gland (bottom) for different draw rates. There is no useful accumulated extensional strain for drawing at 0.1 mm/s. Note that the curves for the two higher drawing rates in the silkworm gland are identical (discussed in text).

process. Analysis of the velocity fields in both glands demonstrates that despite their similarly tapered geometry, the glands produce significantly different velocity fields during flow. These differences in velocity fields induce distinct shear and extensional flow fields. Analysis of the shear and extensional flow fields show that the shear rate and accumulated shear strain reach higher magnitudes in the spider MA gland than the silkworm gland. Additionally, despite a greater magnitude final extension rate in the spider MA gland, the accumulated extensional strain in both organisms is of similar magnitude, suggesting that shear may be the dominant force in inducing the improved mechanical properties of spider silk over silkworm silk. Our results also indicate that the residence time within the spider MA gland is 8-fold greater than in the silkworm gland, allowing greater exposure to shear and extensional fields as well as more time for the diffusion of ions and extraction of water. We furthermore simulated the effect of reeling speed on the flow of silk dope in the gland. Whereas the residence time, shear rate, and extension rate magnitudes are greatly altered by spinning speed, average accumulated shear strain is mostly unaffected. Rather, in the spider MA gland, there is a backward shift in the position where the accumulation of useful extensional strain begins with increasing drawing speed (due to a shift in the location of the critical extension rate threshold along the gland). The silkworm gland, however, generates the same amount of accumulated extensional strain at higher than physiological spinning speeds. These results support, at least in the spider, past suggestions that silk dope detaches from the gland walls into a fiber in response to a critical deformation rate, rather than an accumulated level of strain.

We have discussed the limitations of these simulations in representing in vivo flow characteristics. In particular, future work in measuring the highly extensional character of the silk dope will be critical to developing more realistic models of the in vivo flow of silk solution. Future work will also be required to account for the significant effect of ionic gradients within the gland in altering silk dope viscosity and inducing fiber solidification.

Our results, however, provide an initial step in understanding the role of flow in silk fiber formation, as well as provide insight into the differences between the mechanism of silkworm and spider silk fiber spinning. Studying flow in the 400 million year old,[57] naturally evolved spinnerets of the spider and silkworm glands will assist in the improvement of low energy commercial fiber spinning technologies and the development of new biomimetic systems for fiber spinning.

Acknowledgment. The authors would like to thank Dr. Robert Wootton for helpful discussions and the reviewers for extremely useful comments and suggestions. This research was partially supported by an NDSEG Graduate Fellowship to D.N.B., University of California Systemwide Biotechnology Research and Education Program GREAT Training Grant 2008-02, National Science Foundation Grant No. EEC-0425914, and the Micro/Nano Fluidics Fundamentals Focus (MF3) Center under the DARPA N/MEMS Science and Technology Fundamentals Program.

References and Notes

(1) Vollrath, F.; Knight, D. P. *Nature* **2001**, *410*, 541–8.
(2) Kluge, J. A.; Rabotyagova, O.; Leisk, G. G.; Kaplan, D. L. *Trends Biotechnol.* **2008**, *26*, 244–51.
(3) Asakura, T.; Umemura, K.; Nakazawa, Y.; Hirose, H.; Higham, J.; Knight, D. P. *Biomacromolecules* **2007**, *8*, 175–81.
(4) Dicko, C.; Kenney, J. M.; Vollrath, F. *Adv. Protein Chem.* **2006**, *73*, 17–53.
(5) Kaplan, D.; Adams, W. W.; Farmer, B.; Viney, C. *Silk Polym.* **1994**, *544*, 2–16.
(6) Knight, D. P.; Vollrath, F. *Naturwissenschaften* **2001**, *88*, 179–82.
(7) Foo, C. W. P.; Bini, E.; Hensman, J.; Knight, D. P.; Lewis, R. V.; Kaplan, D. L. *Appl. Phys. A: Mater. Sci. Process.* **2006**, *82*, 223–233.
(8) Willcox, P. J.; Gido, S. P.; Muller, W.; Kaplan, D. L. *Macromolecules* **1996**, *29*, 5106–5110.
(9) Knight, D. P.; Vollrath, F. *Proc. R. Soc. B* **1999**, *266*, 519–523.
(10) Yamaura, K.; Okumura, Y.; Ozaki, A.; Matsuzawa, S. *Appl. Polym. Symp.* **1985**, 205–220.
(11) Holland, C.; Terry, A. E.; Porter, D.; Vollrath, F. *Nat. Mater.* **2006**, *5*, 870–4.
(12) Iizuka, E. *Biorheology* **1966**, *3*, 141–152.
(13) Iizuka, E. *Experientia* **1983**, *39*, 449–454.
(14) Knight, D. P.; Knight, M. M.; Vollrath, F. *Int. J. Biol. Macromol.* **2000**, *27*, 205–10.
(15) Chen, X.; Knight, D. P.; Vollrath, F. *Biomacromolecules* **2002**, *3*, 644–8.
(16) Kojic, N.; Bico, J.; Clasen, C.; McKinley, G. H. *J. Exp. Biol.* **2006**, *209*, 4355–62.
(17) Larson, R. G. *The Structure and Rheology of Complex Fluids*; Oxford University Press: New York, 1999.
(18) Moriya, M.; Ohgo, K.; Masubuchi, Y.; Asakura, T. *Polymer* **2008**, *49*, 952–956.
(19) Doke, J. Mathworks Matlab Central File Exchange, 2005.
(20) Donald, A. M.; Windle, A. H. *Liquid Crystalline Polymers*; Cambridge University Press: Cambridge, England; New York, 1992.
(21) Viney, C. *Supramol. Sci.* **1997**, *4*, 75–81.
(22) Kataoka, K.; Uematsu, I. *Kobunshi Ronbunshu* **1977**, *34*, 37–41.
(23) Shao, Z.; Vollrath, F. *Nature* **2002**, *418*, 741.
(24) Kojic, N.; Kojic, M.; Gudlavalleti, S.; McKinley, G. H. *Biomacromolecules* **2004**, *5*, 1698–707.
(25) Ortlepp, C. S.; Gosline, J. M. *Biomacromolecules* **2004**, *5*, 727–31.
(26) Bird, B.; Hassager, O.; Armstrong, R.; Curtiss, C. *Dynamics of Polymeric Liquids*, 2nd ed.; John Wiley & Sons, Inc: New York, NY, 1987; Vol. 1.
(27) Perkins, T. T.; Smith, D. E.; Chu, S. *Science* **1997**, *276*, 2016–21.
(28) Smith, D. E.; Babcock, H. P.; Chu, S. *Science* **1999**, *283*, 1724–7.
(29) Rammensee, S.; Slotta, U.; Scheibel, T.; Bausch, A. R. *Proc. Natl. Acad. Sci. U.S.A.* **2008**, *105*, 6590–5.

(30) Macosko, C. W.; Larson, R. G. *Rheology: Principles, Measurements, and Applications*; VCH: New York, NY, 1993.
(31) McKinley, G. H.; Sridhar, T. *Annu. Rev. Fluid Mech.* **2002**, *34*, 375–415.
(32) Lee, J. S.; Dylla-Spears, R.; Teclemariam, N. P.; Muller, S. J. *Appl. Phys. Lett.* **2007**, *90*, 074103.
(33) Oliveira, M. S. N.; Alves, M. A.; Pinho, F. T.; McKinley, G. H. *Exp. Fluids* **2007**, *43*, 437–451.
(34) Xie, F.; Zhang, H. H.; Shao, H. L.; Hu, X. C. *Int. J. Biol. Macromol.* **2006**, *38*, 284–288.
(35) James, D. F. *AlChE J.* **1991**, *37*, 59–64.
(36) James, D. F.; Chandler, G. M.; Armour, S. J. *J. Non-Newtonian Fluid Mech.* **1990**, *35*, 421–443.
(37) Holland, C., *Personal Communication*, 2008.
(38) LaNieve, H. U. S. U.S. Patent 3,925,525, 1975.
(39) Chen, G. Y.; Cuculo, J. A.; Tucker, P. A. *J. Polym. Sci., Part B: Polym. Phys.* **1992**, *30*, 557–561.
(40) Crater, D. H.; Cuculo, J. A. *J. Polym. Sci., Part B: Polym. Phys.* **1983**, *21*, 2219–2242.
(41) Anna, S. L.; McKinley, G. H. *Rheol. Acta* **2008**, *47* (8), 841–859.
(42) Lefevre, T.; Boudreault, S.; Cloutier, C.; Pezolet, M. *Biomacromolecules* **2008**, *9*, 2399–2407.
(43) Vollrath, F.; Madsen, B.; Shao, Z. *Proc. Biol. Sci.* **2001**, *268*, 2339–46.
(44) Magoshi, J.; Magoshi, Y.; Nakamura, S. *Appl. Polym. Symp.* **1985**, 187–204.
(45) Guerette, P. A.; Ginzinger, D. G.; Weber, B. H.; Gosline, J. M. *Science* **1996**, *272*, 112–5.
(46) Hinman, M. B.; Lewis, R. V. *J. Biol. Chem.* **1992**, *267*, 19320–4.
(47) Hinman, M.; Dong, Z.; Xu, M.; Lewis, R. V. *Results Probl. Cell Differ.* **1992**, *19*, 227–54.
(48) Sponner, A.; Unger, E.; Grosse, F.; Weisshart, K. *Nat. Mater.* **2005**, *4*, 772–5.
(49) Braun, F. N.; Viney, C. *Int. J. Biol. Macromol.* **2003**, *32*, 59–65.
(50) Johnson, M. A.; Martin, D. C. *Int. J. Biol. Macromol.* **1999**, *24*, 139–144.
(51) De Luca, G.; Rey, A. D. *J. Chem. Phys.* **2006**, *124*, 144904.
(52) Terry, A. E.; Knight, D. P.; Porter, D.; Vollrath, F. *Biomacromolecules* **2004**, *5*, 768–72.
(53) Dicko, C.; Kenney, J. M.; Knight, D. P.; Vollrath, F. *Biochemistry (Moscow)* **2004**, *43*, 14080–7.
(54) Sudarsan, A. P.; Ugaz, V. M. *Lab Chip* **2006**, *6*, 74–82.
(55) Schonfeld, F.; Hardt, S. *AlChE J.* **2004**, *50*, 771–778.
(56) Pathak, J. A.; Ross, D.; Migler, K. B. *Phys. Fluids* **2004**, *16*, 4028–4034.
(57) Shear, W. A.; Palmer, J. M.; Coddington, J. A.; Bonamo, P. M. *Science* **1989**, *246*, 479–481.

BM800752X